Energy Research and Development Division
FINAL PROJECT REPORT

Solar-Reflective "Cool" Walls: Benefits, Technologies, and Implementation

Appendix D: Pedestrian Mean Radiant Temperature and Thermal Comfort (Task 3.1 Report)

California Energy Commission

Gavin Newsom, Governor

Appendix D:
Pedestrian mean radiant temperature and thermal comfort (Task 3.1 report)

Matteo Pizzicotti[1], Ronnen Levinson[2], Nathalie Dumas[1], Benjamin Kurtz[1], Yan Long[1], Negin Nazarian[1], Weilong Zhang[1], Jan Kleissl[1]

[1] Center for Energy Research, University of California, San Diego

[2] Heat Island Group, Lawrence Berkeley National Laboratory

28 February 2018

Abstract

Cool walls affect the thermal environment of pedestrians by (a) increasing shortwave (solar) radiation striking the pedestrian; (b) decreasing longwave (thermal infrared) radiation incident on the pedestrian; and (c) lowering the outside air temperature. Human thermal comfort was quantified through the Standard Equivalent Temperature, SET* for homogeneous neighborhoods of different building types with cool walls. For reference, near a conventional-wall of albedo 0.25 the average diurnal cycle shows a SET* of about 18 ℃ at night and up to 30 ℃ during the day. The pedestrian thermal comfort change due to cool walls is small. During daytime, cool walls raise SET* by up to 0.5 ℃ on average over the year. At night, cool walls lower SET* by up to 0.3 ℃ on average over the year. Since thermal sensation in California is generally too warm the daytime SET* rise corresponds to a slight worsening of thermal comfort. However, the SET* rise is so small that it will go unnoticed by most people. While SET* increases over 0.5 ℃ are occasionally observed, they occur exclusively during clear winter days when the SET* increase is beneficial to pedestrian thermal comfort. SET* differences by building type and climate zone were negligible.

1 Introduction and scope

High albedo ("cool") walls are exterior building walls with surface (usually paint) properties that increase reflection of solar radiation. Albedo is the fraction of incident sunlight reflected, or "solar reflectance", of a material. Cool walls reduce the wall's solar heat gain, which can reduce heat conducted inward through the wall on a hot day, or increase heat conducted outward on a cold day. Cool walls also affect the thermal environment of pedestrians by (a) increasing

shortwave (solar) radiation striking the pedestrian; (b) decreasing longwave (thermal infrared) radiation incident on the pedestrian; and (c) lowering the outside air temperature. The magnitudes of these sometimes-opposing effects on pedestrians are quantified in this report.

The human temperature sensation is approximated through thermal comfort models. Pedestrian thermal comfort depends on clothing and activity as well as meteorological factors including mean radiant temperature (MRT), air temperature, humidity, and wind speed. Raising wall albedo is expected to raise MRT and lower urban air temperature.

MRT and a thermal comfort index are calculated using a building-to-canopy model called TUF-IOBES (Temperature of Urban Facets – Indoor Outdoor Building Energy Simulator). TUF-IOBES simulates heat transfer in a small neighborhood of identical buildings to obtain indoor air, outdoor air, façade, and roof temperatures, and radiative, convective, and conductive heat fluxes. To understand thermal impact on pedestrians, calculations are performed for a person walking near the center of the base of each wall of the central building unit, as shown in Figure 1. Calculations are performed hourly for a typical meteorological year (TMY).
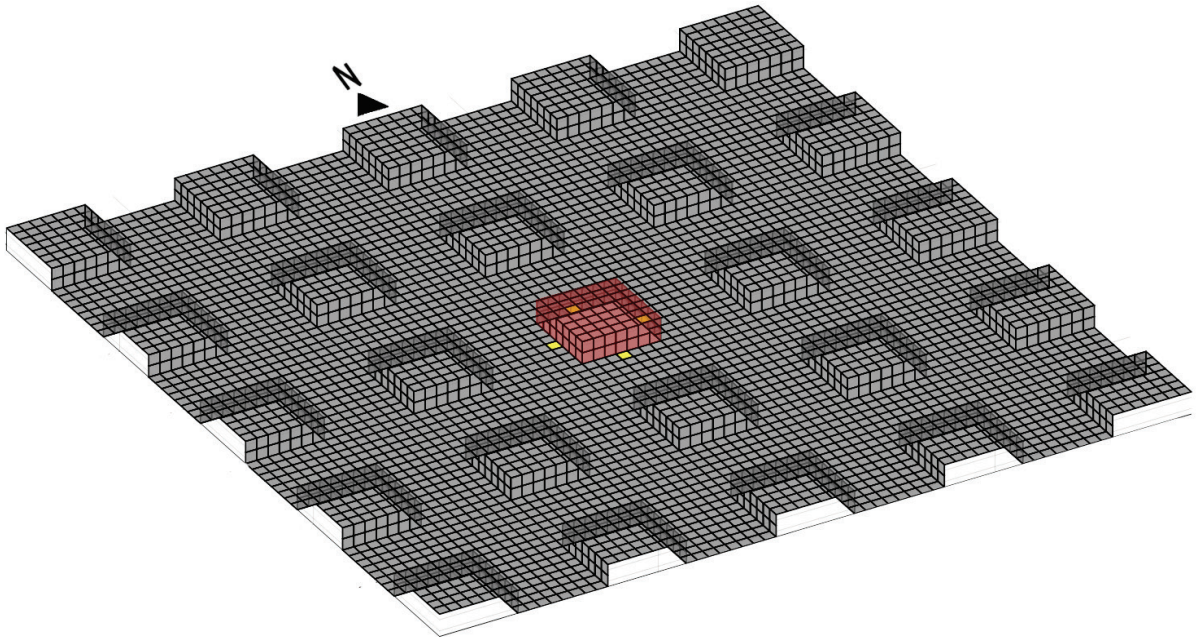
Figure 1. Example of the calculation domain for multi-family residences. The locations of the pedestrian are shown in yellow. The central building unit is highlighted in red.

The results for different California building climate zones (Table 1) and for different building categories (Table 2) will be reported. Three building categories have been chosen that correspond to the most prevalent categories in California: multi-family residence, single-family residence, and medium office building. The climate zones represent a coastal to inland gradient from CZ8 (Fullerton) to CZ10 (Riverside) to CZ13 (Fresno).

Table 1. Climate zones in California with their representative weather stations (California Energy Commission, 2017).

Climate Zone	City	Weather station	Latitude [°N]	Longitude [°W]
CZ8	Fullerton	Fullerton Municipal	33.867	117.983
CZ10	Riverside	Riverside Muni	33.950	117.450
CZ13	Fresno	Fresno-Yosemite-IAP	36.783	119.717

Table 2. Building category and geometrical properties. All facades are identical. *L*, *W*, *H* are building length, width, and height.

Building category	Building footprint dimension $L \times W$ [m × m]	Building height [m]	Building aspect ratio L/H [-]	Ratio of window area to gross wall area [-]	Canyon width [m]	Canyon aspect ratio [-]
Multi-family	27.2 × 27.2	7.8	0.29	0.29	31.1	0.25
Single-family	10.4 × 10.4	5.2	0.50	0.13	28.5	0.18
Medium office	41.6 × 41.6	11.9	0.29	0.32	33.2	0.36

This report is structured as follows. Sections 2 and 3 contain the methodology for the canyon air temperature and MRT calculation. Section 4 contains the methodology for the thermal comfort calculation. Results for different building categories, climate zones, and seasons are presented and discussed in Section 5 separately for mean radiant temperature, canyon air temperature, and thermal comfort. Section 6 concludes the report.

2 Canyon air temperature calculation

In TUF-IOBES, the canyon air temperature is defined as the average temperature of all exterior air space below the building height. Canyon air temperature change is calculated from an energy balance. The control volume is the entire exterior air space below the building height. Heat fluxes into and out of the control volume are (i) convection between canopy air and air above the buildings, in which the air temperature above the buildings is assumed to equal the TMY air temperature; (ii) convection from urban surfaces including pavements and walls; and (iii) heating, ventilation, and air conditioning (HVAC) waste heat.

Switching to cool walls (albedo 0.60, attained with off-white surfaces) from conventional walls (albedo 0.25, typically of dark to medium colors) is expected to lower canyon air temperature. Two factors are at work. First, cool walls absorb less sunlight and remain at a lower temperature than conventional walls. The lower wall temperature reduces convection heat fluxes to the canopy air. Second, building with cool walls require less air conditioning, reducing HVAC waste heat flux into the canyon air.

It is important to disclose a limitation of the TUF-IOBES model. Since the simulation is forced with TMY data above the urban canopy, the canopy air temperature cooling effect of cool walls

is underestimated in TUF-IOBES. A better estimate of city-wide air temperature effects is available in a separate report generated under this contract. However, since these more accurate estimates are only available for two weeks of the year, a comprehensive analysis of seasonal effects was not possible at this time.

3 Mean radiant temperature calculation

3.1 Mean radiant temperature

Mean radiant temperature (MRT) is defined as the uniform surface temperature of an imaginary enclosure in which the human body will exchange the same amount of radiant heat energy as in the actual non-uniform enclosure (ASHRAE Standard 55, 2010). MRT is calculated using the mean radiant flux density (S_{rad}) from the Stefan-Boltzmann equation

$$S_{rad} = \varepsilon_{body}\, \sigma\, T_{MRT}^4, \tag{1}$$

as (VDI 3787 part 2, 2008)

$$T_{MRT} = \sqrt[4]{\frac{S_{rad}}{\varepsilon_{body}\sigma}}, \tag{2}$$

where σ is the Stefan-Boltzmann constant and ε_{body} is the thermal emittance of the human body.

The mean radiant flux density is the mean radiant energy passing through a normal section of the imaginary enclosure per unit time. While radiation is a flux, to make its values more intuitive the flux is expressed as a temperature state utilizing the Stefan-Boltzmann law. The exact threshold for which warm sensation turns into cold sensation depends on the clothing and activity level, but generally if the MRT exceeds the human skin temperature, then a person would experience a warm sensation and vice versa. For an outdoor environment the mean radiant flux density is defined as the summation of shortwave (K) and longwave (L) irradiances weighted by view factors (F) plus the direct contribution from the sun as (VDI 3787 part 2, 2008), such that

$$S_{rad} = \alpha_{SW}\left(\sum_j K_j\, F_{body \to j} + I_d\, F_{sky} + I_b\, f_p\right) + \alpha_{LW}\left(\sum_j L_j\, F_{body \to j} + L_{atm}\, F_{sky}\right), \tag{3}$$

where α_{SW} is the pedestrian's shortwave absorptance and α_{LW} is the pedestrian's longwave absorptance[1]. The index i indexes surfaces including all walls (e.g., the ten walls in Figure 2) and ground. View factors are defined directionally as the fraction of radiation leaving surface A that strikes surface B.
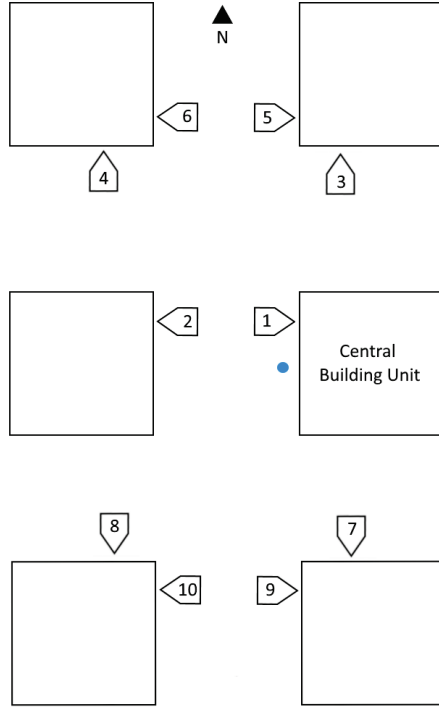
Figure 2. Plan view (not to scale) of a section of the domain identifying the walls that are assumed to contribute to the mean radiant flux. The blue dot to the left of the central building unit locates the pedestrian. Since the domain is symmetric about the center of the central building unit, analogous geometries exist for the other pedestrian locations.

The mean radiant flux density includes the radiation reflected by or emitted from the surrounding surfaces (K_i, L_i); downwelling solar irradiance, both beam (I_b) and diffuse (I_d); and the downwelling atmospheric longwave irradiance (L_{atm}). Shade provided by surrounding buildings is considered by multiplying the beam irradiance (I_b) with a variable that assumes values between 0 (when the patch in which the pedestrian is located is completely shaded) and 1 (when the patch is completely exposed to the sun). The sky and solar terms in Equation (3) are identical for the simulations with different wall albedo. MRT changes resulting from raising wall albedo are solely due to changes in the radiation reflected by or emitted from wall and ground. For simplicity, spatial averages of shortwave and longwave irradiance for each flat surface (i.e., ground, and north, south, east, and west building facades) are used. The radiative

---

[1] By Kirchhoff's law, pedestrian thermal absorptance α_{LW} is equal to pedestrian thermal emittance ε_{body}. The sensitivity of MRT and thermal comfort to pedestrian solar absorptance is analyzed in Section 5.5.

contributions from the façade surfaces (each including walls and windows) of the six buildings surrounding each pedestrian location (Figure 2) are aggregated. Longwave radiation incident on the pedestrian is calculated using wall, window, and ground thermal emittances of 0.90, 0.84, and 0.95, respectively. Conventional (base case) and cool (reflective) walls are assigned albedos (shortwave reflectances) of 0.25 and 0.60, respectively. The albedo of the ground is set to 0.10.

3.2 View factors

The view factor from a person to a surface is the fraction of radiation leaving the person that strikes the surface. The approach by Johnson and Watson (1984) is adopted for view factor calculations. The human body is assumed to be a right circular cylinder with height $H_{body} = 1.8$ m and radius $r = 0.15$ m. The base of the cylinder is on the ground. The cylinder has three surfaces: a circular top plate, a circular bottom plate, and a curved side wall. The view factors from the cylinder surfaces and the entire cylinder to wall, sky, and ground are derived in Task Report Appendix A.

3.3 Solar projection

The surface projection factor for the beam irradiation (I_b) is assumed to be equal to the ratio of A_{sol}, the projection of the human body surface exposed to the solar beam[2], to the total surface area of the human body ($A_{body} = 1.8 \, \text{m}^2$), such that

$$f_p = \frac{A_{sol}}{A_{body}} \tag{4}$$

A_{sol} is calculated using the simplified approach in Underwood et al. (1966)

$$A_{sol} = 0.0429 \, \text{m}^2 \, \sin \alpha_{sol} + 0.3845 \, \text{m}^2 \cos \alpha_{sol}, \qquad [\text{m}^2] \quad (5)$$

where α_{sol} is the solar altitude angle.

3.4 Pedestrian longwave and shortwave absorptances

Longwave absorptances for skin and clothing range from 0.95 to 0.99 and the average of 0.97 is used here (Table 3). Shortwave absorptances vary significantly based on skin color and clothing. The standard shortwave absorptance of 0.70 recommended by Höppe is used here (Table 3), but

---

[2] A_{sol} is the area of the erected human body projected in the direction normal to the solar rays. More intuitively, the A_{sol} is proportional to the length of the shadow of the human body. Per Eq. (5) A_{sol} of a given body depends only the solar altitude angle. A_{sol} decreases with increasing solar altitude angle.

the sensitivity of MRT and thermal comfort to shortwave absorptance is also investigated in Section 5.5.

Table 3. Shortwave and longwave absorptances of skin and clothing (Hoppe, 1992), and the values assigned to the pedestrian.

	Skin	Clothing	Pedestrian
Shortwave absorptance	0.55 to 0.85	0.40 to 0.90	0.70
Longwave absorptance	0.99	0.95	0.97

4 Thermal comfort

MRT is just one input to the thermal comfort of pedestrians. The latest version of the Pierce two-node model (Gagge et al., 1986) is used to compute pedestrian thermal comfort considering MRT, wind speed, air temperature, humidity, metabolic activity, and clothing. Biological and behavioral differences between people make estimation of human comfort more complicated than calculation of MRT, which is derived from first principles in physics. Human comfort models, on the other hand, attempt to emulate the typical human perception of environmental conditions through thermal comfort indices.

Outdoor environmental comfort is more dynamic than indoor comfort, and pedestrians experience a wide range of temperatures. Therefore, body thermoregulatory responses such as shivering and sweating must be considered. The Pierce two-node model captures these responses and is therefore suitable to model outdoor human thermal comfort.

The principal model output is the Standard Equivalent Temperature, SET*. SET* is defined as the air and radiant temperature of a standard isothermal environment that would cause the same thermal stress to the human body as the test environment. A larger SET* indicates that a human feels warmer and vice versa. The human body is modeled as two isothermal concentric compartments, the skin and the core.

The heat balance between the skin and the environment can be written as

$$H_{\mathrm{sk}} = H_{\mathrm{flow}} + Q_{\mathrm{r}} + Q_{\mathrm{c}} + E_{\mathrm{sk}}, \qquad\qquad [\mathrm{W/m^2}] \qquad (6)$$

where H_{sk} is the heat stored in the skin (positive for a body that is heating up), Q_{r} and Q_{c} are the radiative and convective heat losses through skin and clothing, E_{sk} is the evaporative heat loss from the skin, and H_{flow} is heat exchange rate from core to skin. All heat flows and storage are defined per unit area of skin. The heat balance between the skin and the core is

$$H_{\mathrm{cr}} = M - H_{\mathrm{flow}} - (E_{\mathrm{res}} + C_{\mathrm{res}}), \qquad\qquad [\mathrm{W/m^2}] \qquad (7)$$

where H_{cr} is heat stored in the core (positive for a body that is heating up), M is the metabolic activity, and E_{res} and C_{res} are respectively the latent and sensible parts of the respiratory heat losses. To reach thermal equilibrium body thermoregulatory mechanisms, such as vasodilation in warm weather, or vasoconstriction in cold weather, can increase or decrease the heat exchange between core and skin, by adjusting the blood flow rate. If despite adjustments of the blood flow rate, the temperature of the core or skin exceeds a threshold, sweating removes heat. Instead, if the core or skin temperature falls below a threshold, shivering produces additional heat.

Several assumptions about metabolic activity and clothing are needed. A metabolic activity of 115 W/m² corresponding to the heat produced by a person walking on level surface at 3.2 km/h (ASHRAE Standard 55, 2010) is assumed. The insulation provided by clothing is assumed to vary between winter and summer: from November to April, thermal resistance equals 0.155 m² ·K/W, corresponding to trousers, a T-shirt, and a long-sleeve sweater; from May to October, clothing thermal resistance equals 0.088 m²·K/W, corresponding to trousers and a T-shirt (ASHRAE Standard 55, 2010). Heat balances, skin temperature, thermoregulatory strain, and the SET* are calculated as the air and radiant temperature of an isothermal environment with 50% relative humidity and 0.15 m/s wind speed (Gagge et al., 1986) in which the human body would have the same skin temperature and the same thermoregulatory mechanism as in the TUF-IOBES environment.

5 Results and Discussion

5.1 Computed view factors

View factors from the pedestrian to individual building walls, all walls, sky, and ground are reported in Table 4. Note that since windows comprise a portion of the façade area (gross wall area), and window thermal properties are the same for the conventional (albedo 0.25) and cool (albedo 0.60) walls, the view factor from the pedestrian to the modified wall surface is smaller than the façade view factor in Table 4.

For multi-family residence, single-family residence, and medium office building the view factors from the pedestrian to the set of all 10 walls are 34.6%, 29.5%, and 37.9%, respectively. The view factors to the set of all walls are dominated by the view factors to the wall immediately adjacent to the pedestrian which are 30.9%, 27.5%, and 32.1%. View factors to any wall are most sensitive to the distance D of the pedestrian from the wall. Since the adjacent wall (wall 1)

dominates the view factor towards all walls when the pedestrian stands close to it, the view factor to all walls decreases approximately as D^2 following the Nusselt analog for view factors[3].

Table 4. View factor from the pedestrian to each gross wall (façade), sky, and ground by building category. The wall reference numbers are given in Figure 2. By symmetry, the view factors to walls 7, 8, 9, and 10 are equal to those to walls 3, 4, 5, and 6, respectively.

	Multi-family residence	Single-family residence	Medium-office
$F_{body \rightarrow wall,1}$	30.9%	27.5%	32.1%
$F_{body \rightarrow wall,2}$	2.0%	0.7%	3.8%
$F_{body \rightarrow wall,3}$	0.1%	0.3%	0.1%
$F_{body \rightarrow wall,4}$	0.4%	0.2%	0.6%
$F_{body \rightarrow wall,5}$	0.0%	0.0%	0.0%
$F_{body \rightarrow wall,6}$	0.2%	0.1%	0.3%
$F_{body \rightarrow walls}$	33.6%	28.9%	36.9%
$F_{body \rightarrow sky}$	25.0%	29.4%	21.5%
$F_{body \rightarrow ground}$	40.7%	41.1%	40.6%

5.2 Mean Radiant Temperature (MRT)

MRTs for different wall albedos, building types, and climate zones are compared. The multi-family residence in climate zone 8 (Fullerton) with conventional walls (albedo 0.25) is arbitrarily chosen as the reference case.

Figure 3 shows the results averaged over the entire year for the reference case. In TUF-IOBES T_{air} is the forcing (TMY) temperature above the canyon and T_{can} is the simulated air temperature inside the canyon. The MRT follows the trend of air and canyon temperatures, but with larger amplitude. At night T_{MRT} is lower than T_{can} because of the longwave radiation exchanged by the pedestrian with the cool sky and with urban surfaces, which tend to be cooler than the canyon air. During the day T_{MRT} is higher than T_{can} because of beam solar radiation and diffuse solar radiation from the sky, solar radiation reflected by surrounding walls and ground surfaces, and longwave radiation emitted by surrounding walls and ground surfaces. Therefore during the day the only environmental factor that provides sustained radiative cooling is the longwave exchange with the sky.

---

[3] Nusselt (1928) proposed to calculate view factors as the conical projection of the receiving surface on a unit sphere around the emitting surface. The view factor from the emitting surface to the receiving surface is then the fraction of the circle occupied by the conical projection.

The MRT differences between pedestrian locations stem from building shadows, shortwave radiation reflected by walls, and longwave radiation emitted by walls. For example, a pedestrian to the east of the building records higher MRT during the morning in direct sun exposure. A pedestrian to the west of the building is in shadow during the early morning but experiences the highest MRT in the afternoon. The pedestrian in the south location experiences the maximum daily MRT while the pedestrian in the north location experiences the lowest MRT on average. The pedestrian in the north location is often shaded, primarily receiving radiation reflected by and emitted from the north building wall. For example for Fullerton, the north wall only receives 1.3 kWh/m²·day of solar radiation on average during the year, while the south wall receives 3.4 kWh/m²·day of solar radiation.
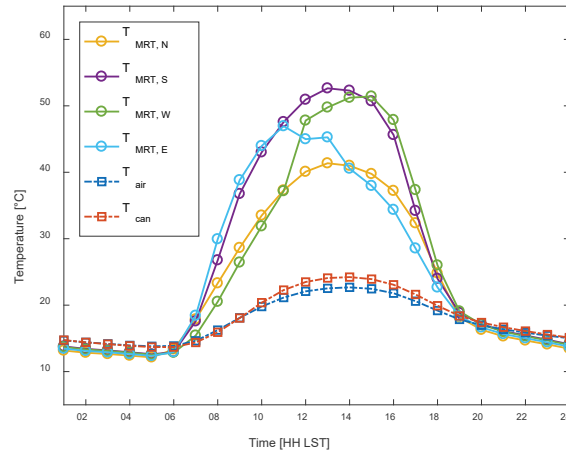
Figure 3. Average (over the year) daily cycle of air and mean radiant temperatures in four locations for the multi-family residence in Fullerton (CZ8) with (conventional) wall albedo equal to 0.25. T_{air} is the forcing air temperature above the urban canopy, T_{can} is the average air temperature in the urban canyon, and $T_{MRT,i}$ is the mean radiant temperature experienced by the pedestrian north, south, west and east of the building (façade i = N, S, W, E). LST is Local Standard Time.
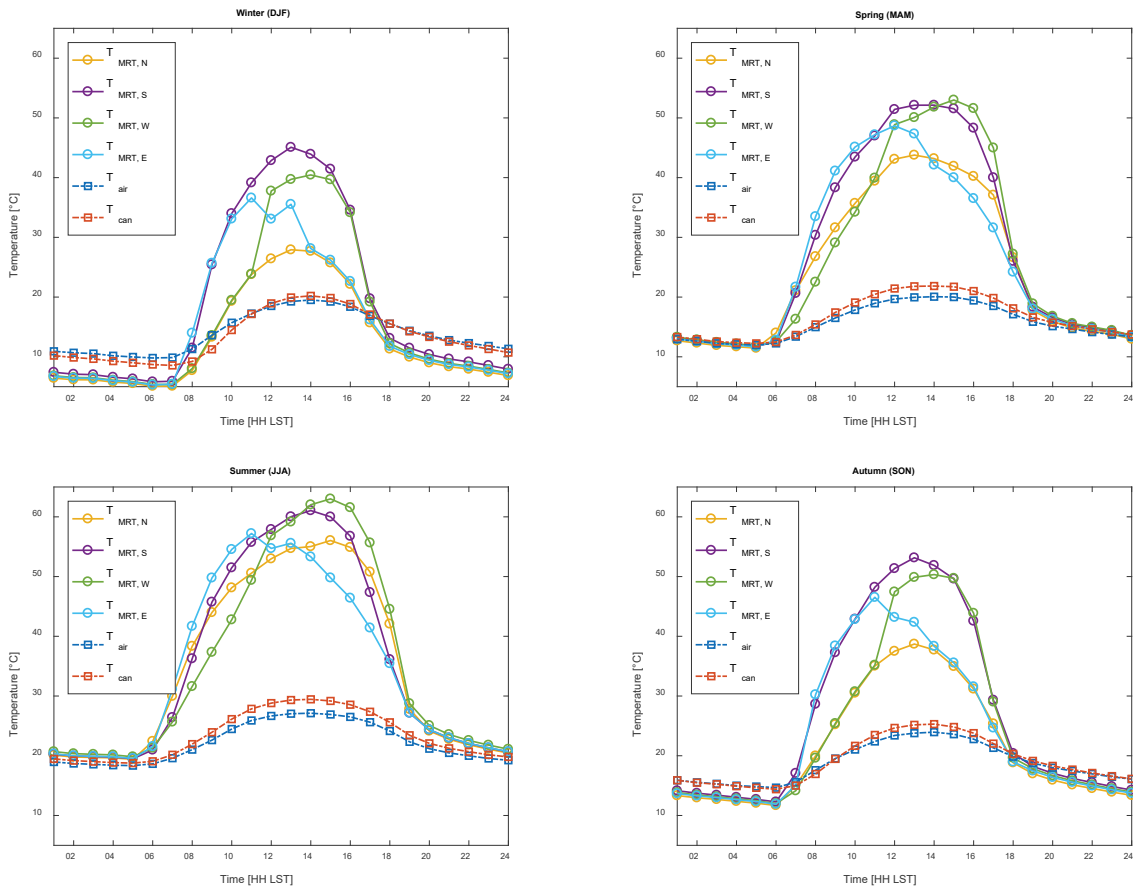
Figure 4. Seasonal analogs of Figure 3 (winter = Dec/Jan/Feb, spring = Mar/Apr/May, summer = Jun/Jul/Aug, and autumn = Sep/Oct/Nov).

MRT differences by building aspect are consistent across the seasons (Figure 4). The MRT for the pedestrian on the west and south sides are largest with seasonally averaged early afternoon peaks up to 63 ℃ in summer and 45 ℃ in winter.

Figure 5 shows the annual average rise in MRT ($\Delta T_{\mathrm{MRT}} = T_{\mathrm{MRT,modified}} - T_{\mathrm{MRT,base}}$) upon switching to a cool wall (albedo 0.60) from a conventional wall (albedo 0.25). Seasonal rises are presented in Figure 6. Increasing wall albedo raises daytime MRT. Compared to a conventional wall, during daytime cool walls reflect a larger fraction of incident solar radiation to the surroundings leading to an increase in pedestrian MRT. While the high albedo also lowers wall surface temperature, the associated reduction in emission of longwave radiation from the wall is not sufficient to balance the shortwave increase. On the other hand, at night the MRT is lower in neighborhoods with cool walls, since a decrease in wall heat storage in cool walls during daytime causes lower wall temperatures to persist through the night. The timing of the peak rise of MRT with wall albedo in Figure 5 depends on pedestrian location and coincides with the MRT peaks in Figure 3.

For any seasonal average and the annual average, the east location experiences the peak MRT rise shortly after sunrise, due to the reflection from the strongly irradiated east facing walls; at the west location the peak MRT rise is recorded just before sunset. The MRT rise at the south and north locations is close to symmetric about noon LST and peaks around noon because of the reflection from the south-facing wall for both locations. The pedestrian near the south wall receives sunlight diffusely reflected from the south wall (pedestrian to south wall view factor 30.9%) that arrived at the south wall as beam radiation from the solar disc. The pedestrian near the north wall receives (i) sunlight diffusely reflected from the north wall (pedestrian to north wall view factor is also 30.9%) that arrived at the north wall as diffuse shortwave radiation from the sky; (ii) sunlight diffusely reflected from the south wall (pedestrian to south wall view factor 2.0%) that arrived at the south wall as beam radiation from the solar disc; (iii) sunlight diffusely reflected from the north wall that arrived at the north wall as diffuse radiation reflected from the south wall (south wall to the north wall view factor 5.6%).

Switching to cool walls from conventional walls increases substantially the shortwave contribution to the MRT, but this is partly offset by a reduction in longwave emission from the now-cooler wall. The pedestrian-to-gross wall view factors are only 33.6% (Table 4), and windows comprise 29% of the façade area (gross wall area) in the multi-family residence, further reducing the view factor from the pedestrian to the modified (net) wall surface area. To illustrate cool wall effects on pedestrian MRT a sample calculation is provided for a clear day on March 22 in Fullerton with a pedestrian walking 1.5 m from a multi-family residence. Daytime mean global horizontal irradiance and mean beam-normal irradiance are 473 W/m^2 and 651 W/m^2, respectively. Averaging over daytime and all walls, switching to cool walls from conventional walls increases reflected radiation to 119 W/m^2 from 49 W/m^2, while decreasing longwave emission to 420 W/m^2 (corresponding to 20.5 ℃) from 444 W/m^2 (24.9 ℃). The net increase in all-wave radiation is 46 W/m^2. However, the change in pedestrian MRT depends also on the pedestrian shortwave absorptance, as analyzed in Section 5.5.
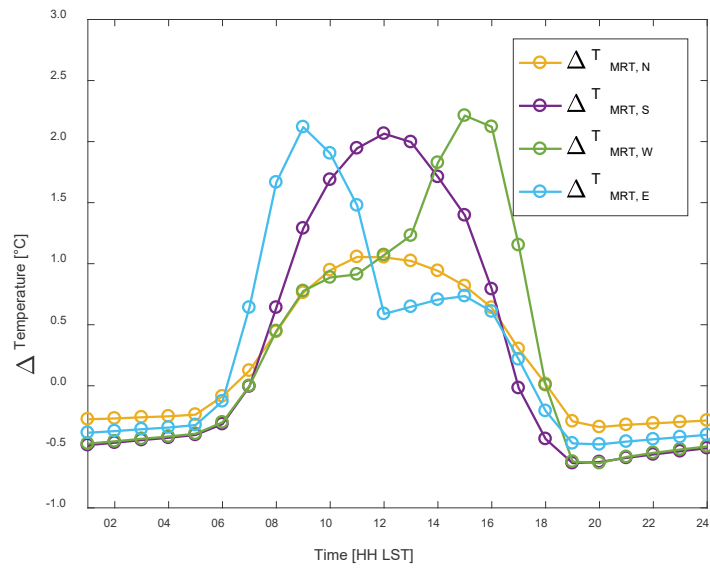
Figure 5. Average (over the year) MRT rise ΔT_{MRT} when switching to cool walls (albedo 0.60) from conventional walls (albedo 0.25) for the multi-family residence in Fullerton (CZ8).
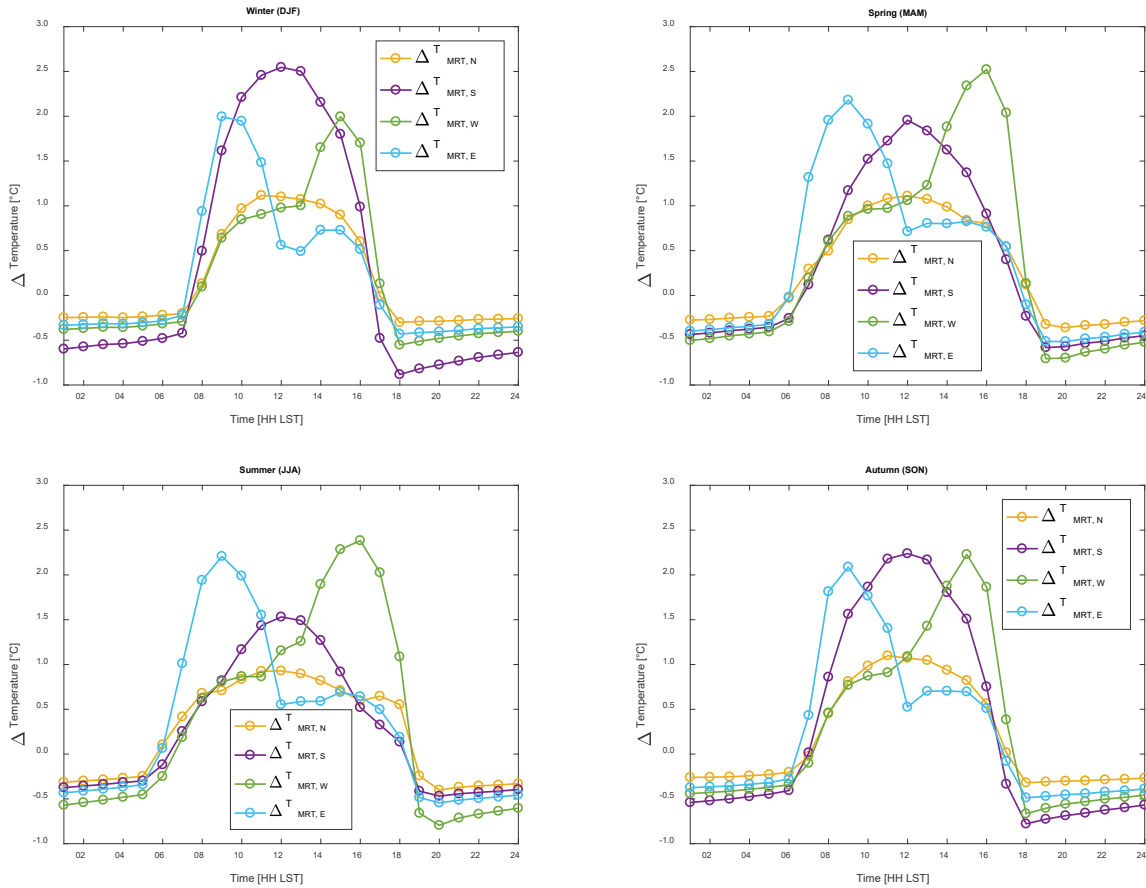
Figure 6. Seasonal analogs of Figure 5 (winter = Dec/Jan/Feb, spring = Mar/Apr/May, summer = Jun/Jul/Aug, and autumn = Sep/Oct/Nov).

The same procedure illustrated above for the multi-family in CZ8 was repeated for the various climate zones and building categories tabulated in Table 1 and Table 2, respectively. The mean MRT and canopy air temperature during the day and the mean daytime increase in MRT and canopy air temperature are shown in Table 5 through Table 13. Section 5.3 discusses the canyon air temperature results.

The earlier finding for the multi-family residence in Fullerton (CZ8) holds for all building categories and climate zones: cool wall MRTs are largest for the pedestrian on the south side, followed by about equal MRT on the east and west sides, and the MRT is lowest for the pedestrian on the north side. The MRT trend with CZ is inconsistent (for examples, see Table 5, Table 6, and Table 7), presumably due to different patterns in the diurnal cycle of cloudiness in the different climate zones. For example the coastal CZ8 tends to be more cloudier in the morning than in the afternoon, especially in summer. Morning cloud cover manifests in a smaller average daily peak MRT for the pedestrian on the east side compared to the west side, because morning cloud cover greatly reduces sunlight incident on the east wall, which in turn reduces reflected sunlight incident on the pedestrian walking next to it. On the other hand, for

CZ10 and CZ13, the average MRT tends to be nearly identical for the pedestrian in the east and west locations, indicating similar solar irradiance for mornings and afternoons.

Pedestrian MRTs are higher in cool-wall neighborhoods with MRT increases ranging from 0.5 to 0.9 °C for a pedestrian at the north wall to 0.6 to 2.0°C for a pedestrian at the south wall depending on season, building type, and climate zone. The largest MRT increases occur on the south wall for the coastal climate zones in the winter.

The results are consistent with the distribution of sunlight on the different facades and seasons. Facades that receive more sunlight also reflect more sunlight toward the pedestrian. As cool walls have larger solar reflectance, they augment this increase in reflection of sunlight to the pedestrian, further increasing MRT. Daytime global irradiance on walls is largest in the winter for the south façade, while it is largest in summer for the east and west façades.

Table 5. Seasonal mean values of daytime canyon air temperature and MRT with conventional walls, and corresponding increases when switching to cool walls (albedo 0.60) from conventional walls (albedo 0.25), shown for the multi-family residence in CZ8. Note that 0.0 is a rounded result with a value between -0.05 °C and 0.05 °C.

	T_{can} [°C]	ΔT_{can} [°C]	$T_{\text{MRT,N}}$ [°C]	$\Delta T_{\text{MRT,N}}$ [°C]	$T_{\text{MRT,S}}$ [°C]	$\Delta T_{\text{MRT,S}}$ [°C]	$T_{\text{MRT,W}}$ [°C]	$\Delta T_{\text{MRT,W}}$ [°C]	$T_{\text{MRT,E}}$ [°C]	$\Delta T_{\text{MRT,E}}$ [°C]
Winter (DJF)	16.6	-0.2	21.0	0.8	33.7	1.6	27.6	1.0	27.1	0.9
Spring (MAM)	19.2	0.0	35.1	0.7	40.5	1.0	38.1	1.2	37.2	1.0
Summer (JJA)	25.9	0.0	45.4	0.6	46.5	0.7	46.2	1.1	44.8	0.9
Autumn (SON)	22.2	-0.1	30.5	0.7	41.5	1.3	36.3	1.1	35.7	1.0
Year	21.3	-0.1	34.1	0.7	41.1	1.1	37.8	1.1	36.9	1.0

Table 6. Analog of Table 5 for multi-family residence in CZ10.

	T_{can} [°C]	ΔT_{can} [°C]	$T_{\text{MRT,N}}$ [°C]	$\Delta T_{\text{MRT,N}}$ [°C]	$T_{\text{MRT,S}}$ [°C]	$\Delta T_{\text{MRT,S}}$ [°C]	$T_{\text{MRT,W}}$ [°C]	$\Delta T_{\text{MRT,W}}$ [°C]	$T_{\text{MRT,E}}$ [°C]	$\Delta T_{\text{MRT,E}}$ [°C]
Winter (DJF)	15.8	-0.1	19.0	0.8	33.2	1.8	26.1	1.1	26.1	1.1
Spring (MAM)	20.2	0.0	36.0	0.7	41.6	1.0	38.9	1.2	38.5	1.1
Summer (JJA)	28.0	0.0	47.0	0.7	48.0	0.8	47.0	1.2	47.0	1.1
Autumn (SON)	22.6	-0.1	28.7	0.7	40.0	1.3	34.2	1.0	34.2	0.9

	T_{can} [°C]	ΔT_{can} [°C]	$T_{MRT,N}$ [°C]	$\Delta T_{MRT,N}$ [°C]	$T_{MRT,S}$ [°C]	$\Delta T_{MRT,S}$ [°C]	$T_{MRT,W}$ [°C]	$\Delta T_{MRT,W}$ [°C]	$T_{MRT,E}$ [°C]	$\Delta T_{MRT,E}$ [°C]
Year	22.1	-0.1	33.9	0.7	41.3	1.2	37.4	1.1	37.3	1.0

Table 7. Analog of Table 5 for multi-family residence in CZ13.

	T_{can} [°C]	ΔT_{can} [°C]	$T_{MRT,N}$ [°C]	$\Delta T_{MRT,N}$ [°C]	$T_{MRT,S}$ [°C]	$\Delta T_{MRT,S}$ [°C]	$T_{MRT,W}$ [°C]	$\Delta T_{MRT,W}$ [°C]	$T_{MRT,E}$ [°C]	$\Delta T_{MRT,E}$ [°C]
Winter (DJF)	11.3	-0.1	16.0	0.7	24.4	1.2	20.3	0.8	20.0	0.8
Spring (MAM)	20.7	0.0	34.3	0.7	40.8	1.1	37.3	1.2	37.3	1.1
Summer (JJA)	31.2	0.0	46.9	0.6	48.2	0.7	47.0	1.1	47.2	1.0
Autumn (SON)	22.3	-0.1	28.7	0.7	41.1	1.4	35.0	1.1	34.8	1.0
Year	22.3	0.0	33.1	0.7	39.7	1.1	36.2	1.0	36.2	1.0

Table 8. Analog of Table 5 for single-family residence in CZ8.

	T_{can} [°C]	ΔT_{can} [°C]	$T_{MRT,N}$ [°C]	$\Delta T_{MRT,N}$ [°C]	$T_{MRT,S}$ [°C]	$\Delta T_{MRT,S}$ [°C]	$T_{MRT,W}$ [°C]	$\Delta T_{MRT,W}$ [°C]	$T_{MRT,E}$ [°C]	$\Delta T_{MRT,E}$ [°C]
Winter (DJF)	16.6	-0.1	21.1	0.6	34.2	1.7	27.9	1.0	28.2	0.9
Spring (MAM)	19.2	0.0	36.9	0.7	41.1	1.0	38.5	1.2	38.0	1.0
Summer (JJA)	25.8	0.0	46.9	0.6	47.7	0.7	46.7	1.1	45.6	0.9
Autumn (SON)	22.2	-0.1	31.5	0.6	41.8	1.4	37.0	1.1	36.9	1.0
Year	21.3	0.0	35.2	0.6	41.7	1.2	38.3	1.1	37.9	0.9

Table 9. Analog of Table 5 for single-family residence in CZ10.

	T_{can} [°C]	ΔT_{can} [°C]	$T_{MRT,N}$ [°C]	$\Delta T_{MRT,N}$ [°C]	$T_{MRT,S}$ [°C]	$\Delta T_{MRT,S}$ [°C]	$T_{MRT,W}$ [°C]	$\Delta T_{MRT,W}$ [°C]	$T_{MRT,E}$ [°C]	$\Delta T_{MRT,E}$ [°C]
Winter (DJF)	15.7	-0.1	19.0	0.7	33.7	2.0	26.5	1.1	27.2	1.1
Spring (MAM)	20.1	0.0	37.8	0.7	42.2	1.1	39.3	1.2	39.1	1.0
Summer (JJA)	28.0	0.0	48.6	0.7	49.4	0.8	47.3	1.2	47.9	1.1

	T_{can} [°C]	ΔT_{can} [°C]	$T_{MRT,N}$ [°C]	$\Delta T_{MRT,N}$ [°C]	$T_{MRT,S}$ [°C]	$\Delta T_{MRT,S}$ [°C]	$T_{MRT,W}$ [°C]	$\Delta T_{MRT,W}$ [°C]	$T_{MRT,E}$ [°C]	$\Delta T_{MRT,E}$ [°C]
Autumn (SON)	22.5	-0.1	29.7	0.6	40.2	1.4	34.9	1.1	35.4	1.0
Year	22.0	-0.1	35.0	0.7	42.0	1.3	37.8	1.1	38.2	1.0

Table 10. Analog of Table 5 for single-family residence in CZ13.

	T_{can} [°C]	ΔT_{can} [°C]	$T_{MRT,N}$ [°C]	$\Delta T_{MRT,N}$ [°C]	$T_{MRT,S}$ [°C]	$\Delta T_{MRT,S}$ [°C]	$T_{MRT,W}$ [°C]	$\Delta T_{MRT,W}$ [°C]	$T_{MRT,E}$ [°C]	$\Delta T_{MRT,E}$ [°C]
Winter (DJF)	11.3	0.0	16.2	0.6	24.6	1.3	20.6	0.8	20.9	0.8
Spring (MAM)	20.7	0.0	36.0	0.7	41.3	1.1	37.5	1.2	38.2	1.1
Summer (JJA)	31.2	0.0	48.4	0.5	49.7	0.7	47.3	1.1	47.9	1.0
Autumn (SON)	22.3	0.0	29.8	0.6	41.2	1.4	35.2	1.1	35.8	1.0
Year	22.3	0.0	34.3	0.6	40.4	1.1	36.5	1.0	37.0	1.0

Table 11. Analog of Table 5 for medium office in CZ8.

	T_{can} [°C]	ΔT_{can} [°C]	$T_{MRT,N}$ [°C]	$\Delta T_{MRT,N}$ [°C]	$T_{MRT,S}$ [°C]	$\Delta T_{MRT,S}$ [°C]	$T_{MRT,W}$ [°C]	$\Delta T_{MRT,W}$ [°C]	$T_{MRT,E}$ [°C]	$\Delta T_{MRT,E}$ [°C]
Winter (DJF)	16.9	-0.2	21.9	0.8	34.6	1.3	28.1	0.9	27.0	0.8
Spring (MAM)	19.5	-0.1	34.5	0.7	40.7	0.9	38.2	1.0	37.3	0.9
Summer (JJA)	26.2	-0.1	44.6	0.6	46.6	0.7	46.4	1.0	45.2	0.8
Autumn (SON)	22.5	-0.1	31.0	0.7	42.2	1.1	36.6	0.9	35.7	0.8
Year	21.6	-0.1	34.0	0.7	41.5	0.9	38.1	1.0	37.0	0.9

Table 12. Analog of Table 5 for medium office in CZ10.

	T_{can} [°C]	ΔT_{can} [°C]	$T_{MRT,N}$ [°C]	$\Delta T_{MRT,N}$ [°C]	$T_{MRT,S}$ [°C]	$\Delta T_{MRT,S}$ [°C]	$T_{MRT,W}$ [°C]	$\Delta T_{MRT,W}$ [°C]	$T_{MRT,E}$ [°C]	$\Delta T_{MRT,E}$ [°C]
Winter (DJF)	15.9	-0.2	20.0	0.9	34.0	1.5	26.7	1.0	25.9	0.9
Spring (MAM)	20.4	-0.1	35.4	0.7	41.9	0.9	38.9	1.0	38.6	1.0

	T_{can} [°C]	ΔT_{can} [°C]	$T_{MRT,N}$ [°C]	$\Delta T_{MRT,N}$ [°C]	$T_{MRT,S}$ [°C]	$\Delta T_{MRT,S}$ [°C]	$T_{MRT,W}$ [°C]	$\Delta T_{MRT,W}$ [°C]	$T_{MRT,E}$ [°C]	$\Delta T_{MRT,E}$ [°C]
Summer (JJA)	28.4	-0.1	46.2	0.7	48.0	0.7	47.2	1.1	47.3	1.0
Autumn (SON)	22.7	-0.1	29.2	0.7	40.6	1.1	34.3	0.9	34.3	0.8
Year	22.3	-0.1	33.8	0.7	41.7	1.0	37.6	1.0	37.4	0.9

Table 13. Analog of Table 5 for medium office in CZ13.

	T_{can} [°C]	ΔT_{can} [°C]	$T_{MRT,N}$ [°C]	$\Delta T_{MRT,N}$ [°C]	$T_{MRT,S}$ [°C]	$\Delta T_{MRT,S}$ [°C]	$T_{MRT,W}$ [°C]	$\Delta T_{MRT,W}$ [°C]	$T_{MRT,E}$ [°C]	$\Delta T_{MRT,E}$ [°C]
Winter (DJF)	11.5	-0.1	16.8	0.6	25.1	1.0	20.7	0.7	19.9	0.7
Spring (MAM)	21.0	-0.1	33.8	0.7	41.2	0.9	37.6	1.0	37.4	1.0
Summer (JJA)	31.6	-0.1	46.1	0.6	48.5	0.6	47.4	1.0	47.5	0.9
Autumn (SON)	22.6	-0.1	29.3	0.7	41.8	1.1	35.4	0.9	34.3	0.9
Year	22.6	-0.1	33.0	0.7	40.2	0.9	36.6	0.9	36.2	0.9

5.3 Canyon Air Temperature

Canopy air temperature was reported in the figures and tables in Section 5.2 together with MRT and the trends are briefly summarized here. As expected canopy air temperatures increase along the gradient from coast to inland from CZ8 to CZ10 to CZ13, and the amplitude of the seasonal cycle is also larger inland. Average yearly canopy air temperatures range from 21.3 ℃ to 22.6 ℃. Average yearly canopy air temperatures for the conventional wall case are about 0.3 ℃ higher for the medium office building than for the residential buildings, since the larger building height for the medium office building compared to the residential buildings provides more wall surface area for solar radiation to be absorbed. Canopy air temperature then increases by convection of heat from walls.

Canopy air temperatures are up to 0.2 ℃ lower in cool wall neighborhoods compared to neighborhoods with conventional walls. The largest canopy air temperature reductions of 0.2 ℃ occur for the multi-family residence and medium office building in CZ8 during winter. All other buildings, climate zones, and seasons show cooler canyon air temperature by either 0.0 or 0.1 ℃. Canyon air temperature differences being largest in winter is inconsistent with the fact that total irradiation received on all four walls in winter is only about half that received during summer. More wall irradiation should lead to more reflection of sunlight out of the urban canyon and a larger canyon air temperature difference for cool versus conventional walls. The reason for the discrepancy is not well understood at present.

5.4 Thermal Comfort

The thermal comfort trends during the day follow the MRT and canopy air temperature trends. SET* differences between the simulations with wall albedos of 0.25 (conventional) and 0.60 (cool) can only be due to differences in MRT and canopy air temperature because the other meteorological parameters (i.e., relative humidity and wind speed) are identical. SET* differences between the four pedestrian locations are solely explained by MRT differences as air temperature and other meteorological parameter are assumed to be constant in the domain.

Figure 7 shows SET* for the reference case (a conventional-wall multi-family residence in Fullerton) averaged over the year. At night the SET* is on average around 3 °C higher than the canyon air temperature (Figure 3). While the MRT is lower than the canyon air temperature cooling the pedestrian, the fact that the pedestrian produces heat through walking introduces an overall warmer thermal sensation than the canyon air temperature. During the day the SET* is up to 7 °C higher than the canyon air temperature; the increase is caused by (i) heat production through walking and (ii) a larger MRT. The SET* trends by pedestrian location mirror those for MRT in Figure 3. Figure 8 shows the results by season which exhibit similar trends as those for the entire year.
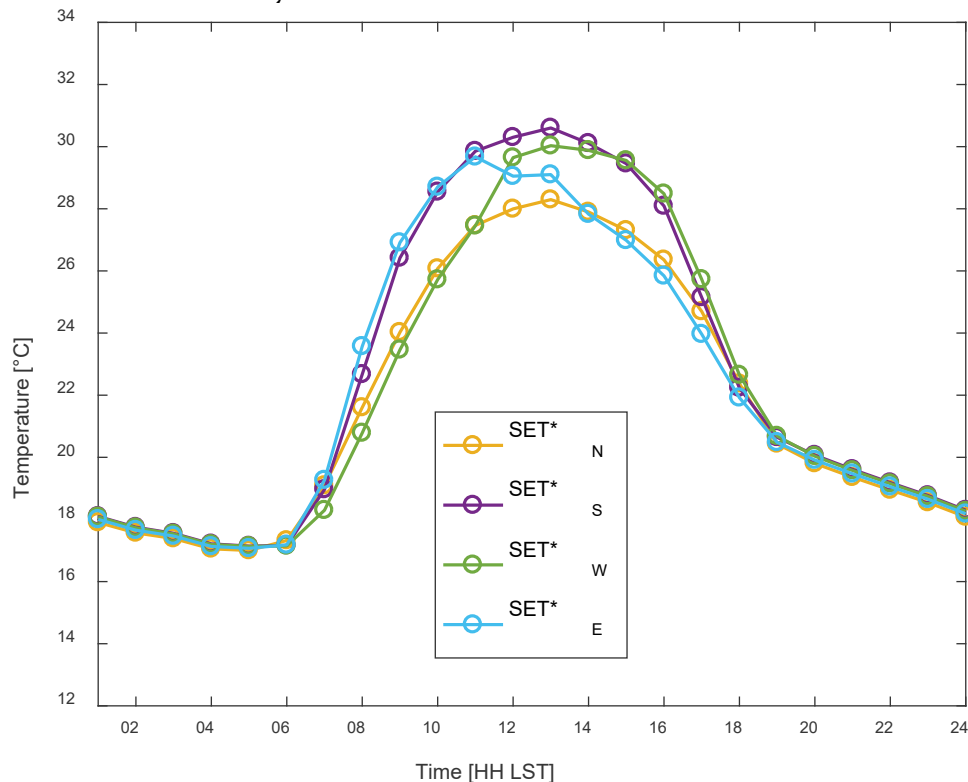
Figure 7. Average (over the year) daily cycle of SET* in four pedestrian locations for the conventional-wall multi-family residence in Fullerton (CZ8).
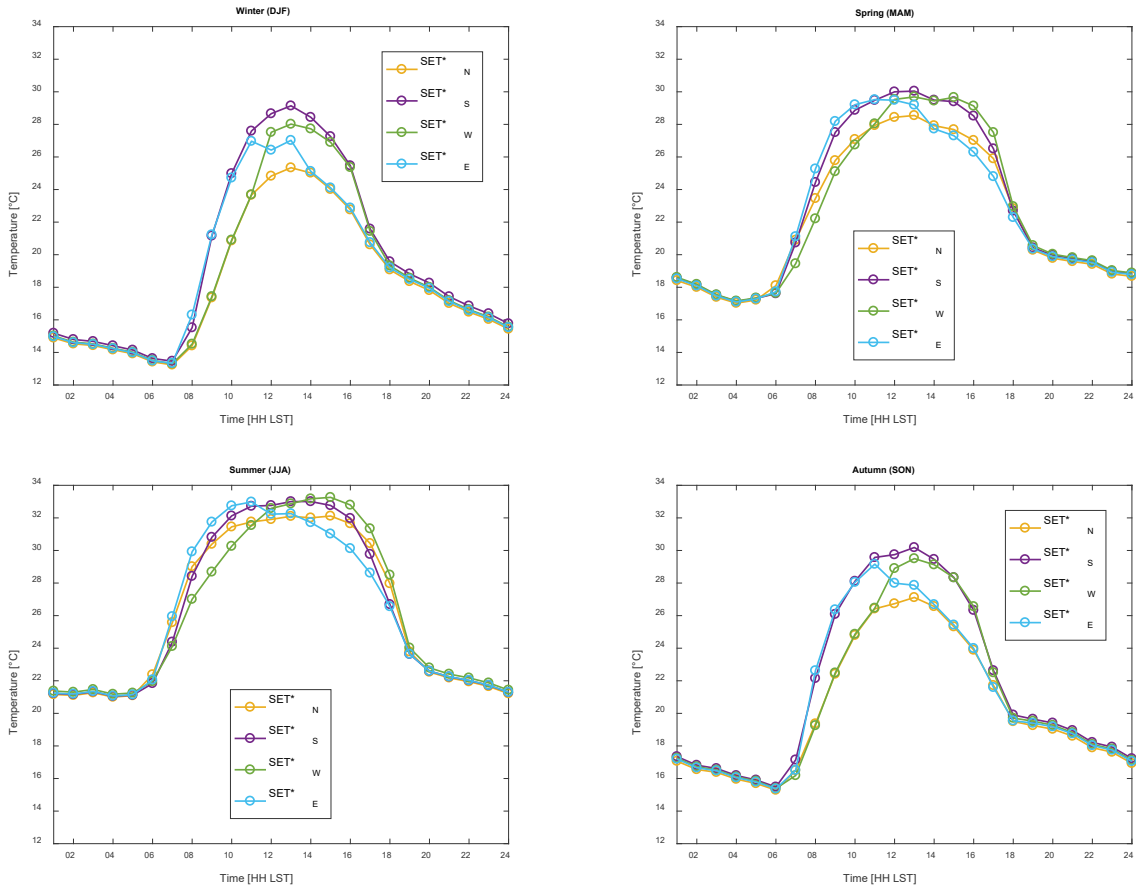
Figure 8. Seasonal analogs of Figure 7 (winter = Dec/Jan/Feb, spring = Mar/Apr/May, summer = Jun/Jul/Aug, and autumn = Sep/Oct/Nov).

As shown in Figure 9 and Figure 10 the pedestrian thermal comfort impact of cool walls is small. During daytime, cool walls increase MRT (Table 5 to Table 13), raising SET* by up to 0.5 ˚C on average over the season or year. At night, cool walls decrease MRT, lowering SET* by up to 0.3 ˚C on average over the season or year. The largest SET* effect occurs for the pedestrian near the south wall in winter since winter solar irradiation on the south wall is the most of any wall during any season. The increase in SET* is only about 0.25 ˚C per 1 ˚C increase in MRT, since the MRT increase due to the higher wall albedo is partially balanced by a decrease in canopy air temperature.
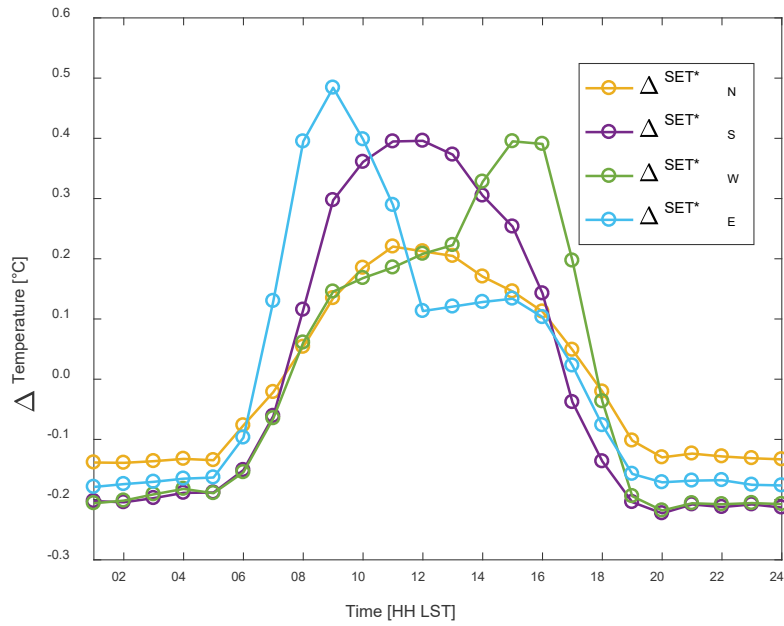
Figure 9. Average (over the year) SET* rise ΔSET* when switching to cool walls (albedo 0.60) from conventional walls (albedo 0.25) for the multi-family residence in Fullerton (CZ8).
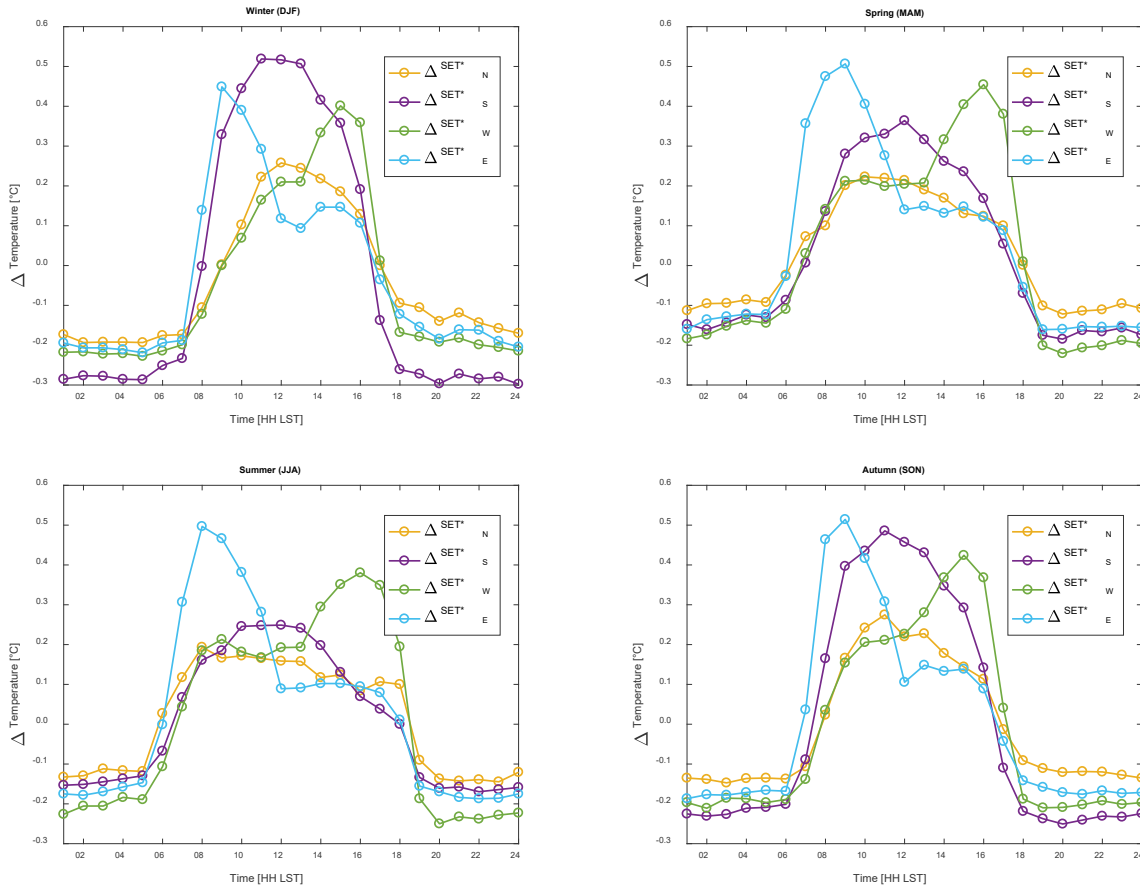
Figure 10. Seasonal analogs of Figure 9 (winter = Dec/Jan/Feb, spring = Mar/Apr/May, summer = Jun/Jul/Aug, and autumn = Sep/Oct/Nov).

For the multi-family residence in Fullerton (CZ8) and all pedestrian locations the absolute SET* difference with cool walls is less or equal to 0.2 °C 61% of the time (Figure 11 and Figure 12). While SET* increases over 0.5 °C are occasionally observed, they occur exclusively during clear winter days when the pedestrian is more likely to experience a cold sensation. In that situation the SET* increase is beneficial to pedestrian thermal comfort.
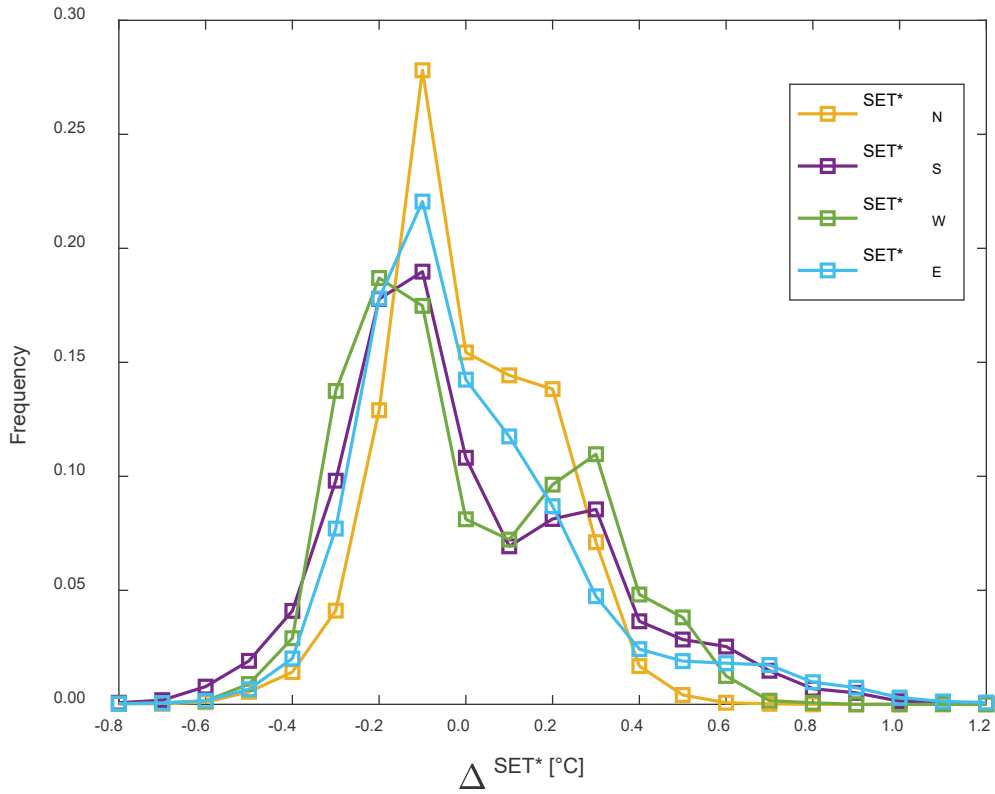
Figure 11. Frequency distribution of standard equivalent temperature (SET*) rise for pedestrians when switching to cool walls (albedo 0.60) from conventional walls (albedo 0.25). Results are for the multi-family residence in Fullerton (CZ8) and the entire year.
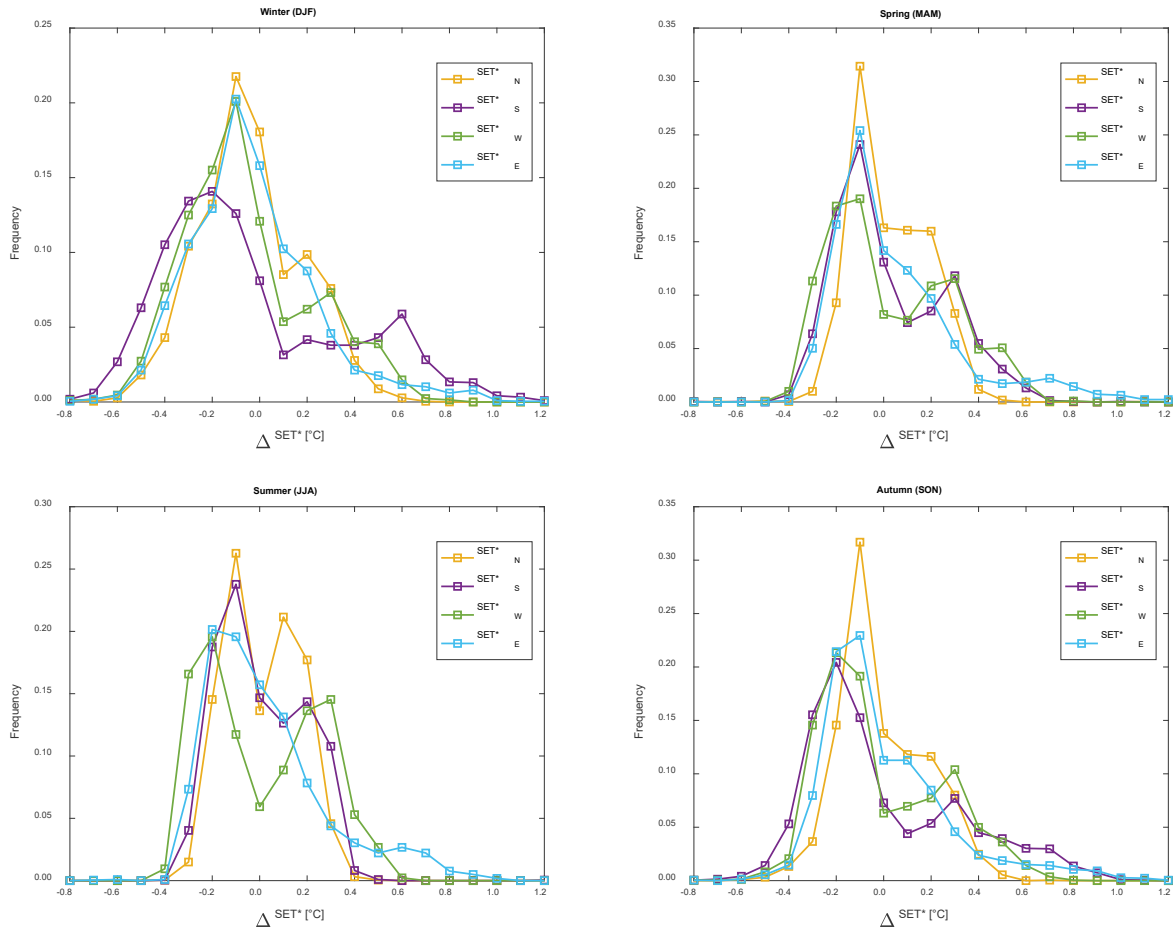
Figure 12. Seasonal analogs of Figure 11 (winter = Dec/Jan/Feb, spring = Mar/Apr/May, summer = Jun/Jul/Aug, and autumn = Sep/Oct/Nov).

As before for the MRT, the mean increase of SET* for a pedestrian near a cool wall during daytime in the entire year is reported in Table 14 through Table 22 for the different building types and climate zones. The average SET* increase ranges from 0.1 ˚C to 0.4 ˚C and is smallest for the north wall, in the summer, for the inland climate zone (CZ13), or the medium office building.

The SET* increase patterns follow the MRT trends, since MRT is an input to SET*. But SET* rises only about 0.25 ˚C per 1 ˚C increase in MRT, because SET* also depends on the canopy air temperature. Since canopy air temperature changes are 0.2˚C or less for all but two winter results, the canopy air temperature effects are less influential than the MRT effects.

Table 14. Rise in mean annual Standard Equivalent Temperature (SET*) induced by switch to cool walls from conventional walls, shown for the multi-family residence in CZ8.

	ΔSET_N^* [°C]	ΔSET_S^* [°C]	ΔSET_W^* [°C]	ΔSET_E^* [°C]
Winter (DJF)	0.1	0.3	0.2	0.2
Spring (MAM)	0.1	0.2	0.2	0.2
Summer (JJA)	0.1	0.1	0.2	0.2
Autumn (SON)	0.1	0.3	0.2	0.2
Year	0.1	0.2	0.2	0.2

Table 15. Analog of Table 14 for the multi-family residence in CZ10.

	ΔSET_N^* [°C]	ΔSET_S^* [°C]	ΔSET_W^* [°C]	ΔSET_E^* [°C]
Winter (DJF)	0.1	0.3	0.2	0.2
Spring (MAM)	0.1	0.2	0.2	0.2
Summer (JJA)	0.1	0.1	0.2	0.2
Autumn (SON)	0.1	0.2	0.2	0.2
Year	0.1	0.2	0.2	0.2

Table 16. Analog of Table 14 for the multi-family residence in CZ13.

	ΔSET_N^* [°C]	ΔSET_S^* [°C]	ΔSET_W^* [°C]	ΔSET_E^* [°C]
Winter (DJF)	0.1	0.3	0.2	0.2
Spring (MAM)	0.1	0.2	0.2	0.2
Summer (JJA)	0.1	0.1	0.1	0.2
Autumn (SON)	0.1	0.3	0.2	0.2
Year	0.1	0.2	0.2	0.2

Table 17. Analog of Table 14 for the single-family residence in CZ8.

	ΔSET_N^* [°C]	ΔSET_S^* [°C]	ΔSET_W^* [°C]	ΔSET_E^* [°C]
Winter (DJF)	0.1	0.4	0.2	0.2
Spring (MAM)	0.1	0.2	0.2	0.2
Summer (JJA)	0.1	0.1	0.2	0.2
Autumn (SON)	0.1	0.3	0.2	0.2
Year	0.1	0.2	0.2	0.2

Table 18. Analog of Table 14 for the single-family residence in CZ10.

	ΔSET_N^* [°C]	ΔSET_S^* [°C]	ΔSET_W^* [°C]	ΔSET_E^* [°C]
Winter (DJF)	0.1	0.4	0.2	0.3
Spring (MAM)	0.2	0.2	0.2	0.3
Summer (JJA)	0.1	0.1	0.2	0.2
Autumn (SON)	0.1	0.3	0.2	0.2
Year	0.1	0.3	0.2	0.2

Table 19. Analog of Table 14 for the single-family residence in CZ13.

	ΔSET_N^* [°C]	ΔSET_S^* [°C]	ΔSET_W^* [°C]	ΔSET_E^* [°C]
Winter (DJF)	0.1	0.3	0.2	0.2
Spring (MAM)	0.1	0.2	0.2	0.2
Summer (JJA)	0.1	0.1	0.1	0.2
Autumn (SON)	0.1	0.3	0.2	0.2
Year	0.1	0.2	0.2	0.2

Table 20. Analog of Table 14 for the medium office in CZ8.

	ΔSET_N^* [°C]	ΔSET_S^* [°C]	ΔSET_W^* [°C]	ΔSET_E^* [°C]
Winter (DJF)	0.1	0.2	0.1	0.1
Spring (MAM)	0.1	0.1	0.2	0.2
Summer (JJA)	0.1	0.1	0.2	0.2
Autumn (SON)	0.1	0.2	0.2	0.2
Year	0.1	0.2	0.2	0.2

Table 21. Analog of Table 14 for the medium office in CZ10.

	ΔSET^*_N [°C]	ΔSET^*_S [°C]	ΔSET^*_W [°C]	ΔSET^*_E [°C]
Winter (DJF)	0.1	0.2	0.1	0.1
Spring (MAM)	0.1	0.1	0.2	0.2
Summer (JJA)	0.1	0.1	0.2	0.2
Autumn (SON)	0.1	0.2	0.1	0.1
Year	0.1	0.2	0.1	0.2

Table 22. Analog of Table 14 for the medium office in CZ13.

	ΔSET^*_N [°C]	ΔSET^*_S [°C]	ΔSET^*_W [°C]	ΔSET^*_E [°C]
Winter (DJF)	0.1	0.2	0.1	0.1
Spring (MAM)	0.1	0.1	0.1	0.2
Summer (JJA)	0.1	0.1	0.1	0.1
Autumn (SON)	0.1	0.2	0.1	0.1
Year	0.1	0.1	0.1	0.1

5.5 Sensitivity to pedestrian shortwave absorptance

Pedestrian shortwave absorptance (α_k) is a parameter that can change considerably between persons (Table 3) due to differences in skin and clothing colors. A sensitivity analysis for MRT and thermal comfort to α_k is performed for the pedestrian near the multi-family residence in Fullerton. While α_k was 0.70 in the preceding analysis, here the project team also reports results for $\alpha_k = 0.40$ (light-colored clothing and/or skin) and $\alpha_k = 0.90$ (dark clothing and/or skin). The results are reported as the average daily cycle of MRT and SET* for the pedestrian at the south of the building. As expected pedestrian MRT is most sensitive to α_k during midday when solar radiation incident on the south wall peaks. Increase absorption of solar radiation (higher α_k) boosts the rise in MRT upon switching to cool walls. MRT differences for the light and dark-colored pedestrian with respect to the case with $\alpha_k = 0.70$ range between -1.4 ˚C and +0.8 ˚C, on

average. Notably even the light-colored pedestrian experiences a MRT increase during most of the daytime. The results by season are similar to those in Figure 6 and are not shown.
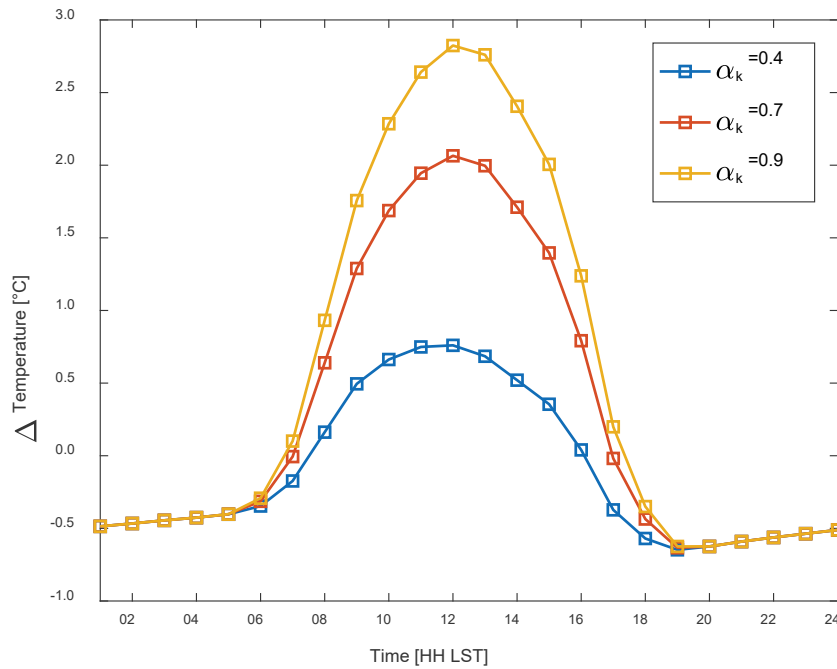
Figure 13. Average (over the year) T_{MRT} rise upon switching to cool walls (albedo 0.60) from conventional walls (albedo 0.25). Result are for the multi-family residence in Fullerton (CZ8) for a pedestrian at the south location for different values of pedestrian shortwave absorptance α_{k}. Refer to Figure 5 for results for the pedestrian with $\alpha_{\mathrm{k}}. = 0.70$ standing near the other walls.

The SET* sensitivity to α_{k} in Figure 14 is similar to the MRT sensitivity. The SET* sensitivity is smaller than the MRT sensitivity because the MRT is only one of the inputs to the SET* while the other inputs are unaffected by α_{k}. On average, relative to the pedestrian with $\alpha_{\mathrm{k}} = 0.7$, SET* is up to 0.13 ˚C higher for a pedestrian with $\alpha_{\mathrm{k}} = 0.90$ and up to 0.25 ˚C lower for a pedestrian with $\alpha_{\mathrm{k}} = 0.40$. For the pedestrian with low solar absorptance (light-colored clothing and/or skin), the 24 h averaged effect of cool walls is a cooler thermal sensation as the daytime warmer thermal sensation is offset by a colder thermal sensation at night.
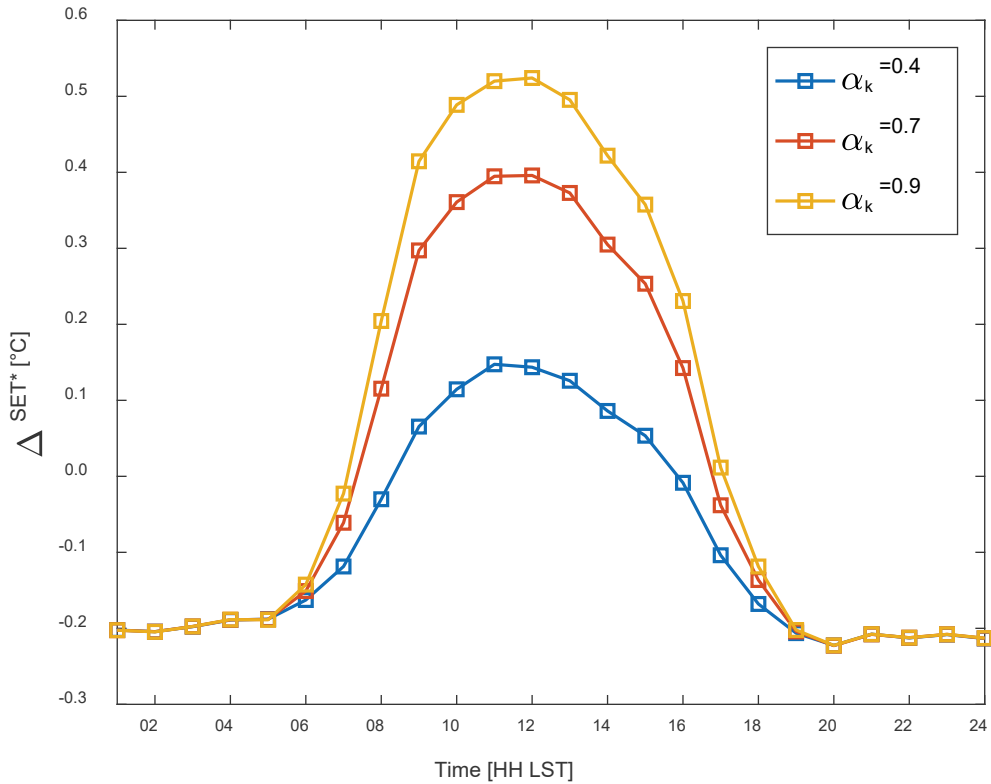
Figure 14. Average (over the year) SET* rise upon switching to cool walls (albedo 0.60) from conventional walls (albedo 0.25). Results are for the multi-family residence in Fullerton (CZ8) for a pedestrian at the south location for different α_k.

6 Conclusions and Limitations

MRT and thermal comfort were analyzed for homogeneous neighborhoods of either multi-family residences, single-family residences, or medium office buildings with cool walls. Typical meteorological year weather data is input to a neighborhood heat transfer model (TUF-IOBES) in three different California climate zones to understand impacts on a pedestrian walking 1.5 m away from walls at the four cardinal orientations. The typical daytime MRT rise near a cool wall (albedo of 0.60) versus a conventional wall (albedo of 0.25) is around 1 °C in most cases. Maximum rise occurred for a pedestrian near the south wall in winter and minimum rise occurred for a pedestrian near the north wall. MRT differences by building type and climate zone were negligible.

Cool walls bring about an average increase in daytime standard equivalent temperature (a measure of thermal comfort) of 0.4 °C or less at all pedestrian locations, building types, and climate zones. Since thermal sensation in California is generally too warm this corresponds to a

slight worsening of thermal comfort. However, the largest standard equivalent temperature increases occur in winter when a cold thermal sensation is more common. During winter, cool walls therefore improve thermal comfort. The results are sensitive to the pedestrian solar absorptance; a pedestrian with extremely small solar absorptance may even experience a cooler thermal comfort, on average over the year.

As described in Section 2, since the TUF-IOBES simulation is forced with TMY data above the urban canopy, the canopy air temperature cooling effect of cool walls is underestimated in TUF-IOBES. The project team projects that actual daytime thermal comfort temperature increases would be less than the 0.4 ℃ estimated here.

7 References

ASHRAE. 2010. Standard 55-2010: Thermal Environmental Conditions for Human Occupancy. Atlanta USA.

California Energy Commission. 2017. California Energy Maps. http://www.energy.ca.gov/maps/renewable/building_climate_zones.html. Accessed May 15, 2017.

Gagge AP, Fobelets AP, Berglund L. 1986. A standard predictive index of human response to the thermal environment. *ASHRAE Transactions* 92(2), 709-731.

Höppe P. 1992. Ein neues Verfahren zur Bestimmung der mittleren Strahlungstemperatur im Freien. *Wetter und Leben* 44(1-3), 147-151 (in German). Translation: Title: A new method for determining exterior mean radiant temperature.

Johnson GT, Watson ID. 1984. Person view-factors in the urban environment. *Meteorology and Atmospheric Physics* 34(3), 273-285. https://doi.org/10.1007/BF02265493

Nusselt, W., 1928. Grafische Bestimmung des Winkelverhaltnisses bei der Warmestrahlung. *Zeitschrift des Vereines Deutscher Ingenieure*, 72(20), p.673. Translation: Title: Graphical view factor determination in heat transfer.

Rosado, PJ. 2016. Evaluating cool impervious surfaces: application to an energy-efficient residential roof and to city pavements. Ph.D. Dissertation, University of California at Berkeley. http://escholarship.org/uc/item/6bf80485.

Underwood C R, Ward E J. 1966. The solar radiation area of man. *Ergonomics* 9(2), 155-168. http://doi.org/10.1080/00140136608964361

VDI. 2008. VDI 3787 part 2: Environmental meteorology - Methods for the human biometeorological evaluation of climate and air quality for urban and regional planning at regional level. Düsseldorf Germany. http://www.vdi.eu/nc/guidelines/vdi_3787_blatt_2-

umweltmeteorologie_methoden_zur_human_biometeorologischen_bewertung_von_klima_und_l
ufthy_/

Task Report Appendix A: View factors

A.1. View factors from curved side wall

A.1.1. Calculating cylinder side wall view factor from slice side wall view factors

To prepare to calculate view factors from the cylinder's side wall to building walls, sky, and ground, we divide the cylinder's side wall (surface C) of area $A_C = 2\,\pi\,r\,H_{\text{body}}$ into a series of M thin horizontal slices of thickness Δh and area $A_{\Delta C} = 2\,\pi\,r\,\Delta h$.

If the view factor from some surface B (building wall, sky, or ground) to the cylinder's side wall of slice i at height h_i (surface ΔC_i) is $F_{\text{B}\to\Delta\text{C},i}$, the view factor from surface B to surface C will be

$$F_{\text{B}\to\text{C}} = \sum_{i=1}^{M} F_{\text{B}\to\Delta\text{C},i}\ . \tag{A-8}$$

Applying the view factor reciprocity relationship

$$A_{\text{X}}F_{\text{X}\to\text{Y}} = A_{\text{Y}}F_{\text{Y}\to\text{X}} \tag{A-9}$$

to each side of Eq. (A-8) yields

$$\frac{A_C}{A_B}F_{\text{C}\to\text{B}} = \sum_{i=1}^{M} \frac{A_{\Delta C}}{A_B} F_{\Delta\text{C},i\to\text{B}}. \tag{A-10}$$

Rearranging,

$$F_{\text{C}\to\text{B}} = \frac{1}{A_C}\sum_{i=1}^{M} F_{\Delta\text{C},i\to\text{B}}\, A_{\Delta C} = \frac{1}{2\,\pi\,r\,H_{\text{body}}}\sum_{i=1}^{M} F_{\Delta\text{C},i\to\text{B}}\, 2\,\pi\,r\,\Delta h\ . \tag{A-11}$$

Transforming the sum to an integral,

$$F_{\text{C}\to\text{B}} = \frac{1}{H_{\text{body}}}\sum_{i=1}^{M} F_{\Delta\text{C},i\to\text{B}}\,\Delta h = \frac{1}{H_{\text{body}}}\int_0^{H_{\text{body}}} F_{\Delta\text{C}\to\text{B}}(h)\,dh = \overline{F_{\Delta\text{C}\to\text{B}}}\ , \tag{A-12}$$

where the bar operator signifies averaging over all slices. In other words, the view factor from the side wall of the cylinder to some surface B is the average of the view factors from the side walls of its slices to surface B.

A.1.2. View factor from cylinder side wall to building wall

Now consider radiative exchange between a slice side wall ΔC and the building wall of height H shown in Figure A-1. The view factors from the cylinder's slice side wall to the portion of

the building wall above the slice ("upper building wall", or UBW), and to the portion of the building wall below the slice ("lower building wall", or LBW), are

$$F_{\Delta C \to UBW} = \frac{1}{\pi^2} \int_{\gamma_1}^{\gamma_2} \int_0^{\omega_1} \cos^2 \phi \, d\phi \, d\theta \tag{A-13}$$

and

$$F_{\Delta C \to LBW} = \frac{1}{\pi^2} \int_{\gamma_1}^{\gamma_2} \int_{\omega_2}^0 \cos^2 \phi \, d\phi \, d\theta , \tag{A-14}$$

respectively. Here θ is the angle in the horizontal plane and the integration is from γ_1 to γ_2 which are the angles in the horizontal plane between the normal to the wall and the left and right edges of the wall, respectively. ϕ is the angle in the vertical plane and the integration bounds are ω_1 and ω_2, which are the angles between the horizontal plane containing ΔC and the top and bottom edge of the wall, respectively. Therefore $\omega_1 = \tan^{-1}\left(\frac{H-h}{D}\cos\theta\right)$ and $\omega_2 = -\tan^{-1}\left(\frac{h}{D}\cos\theta\right)$.
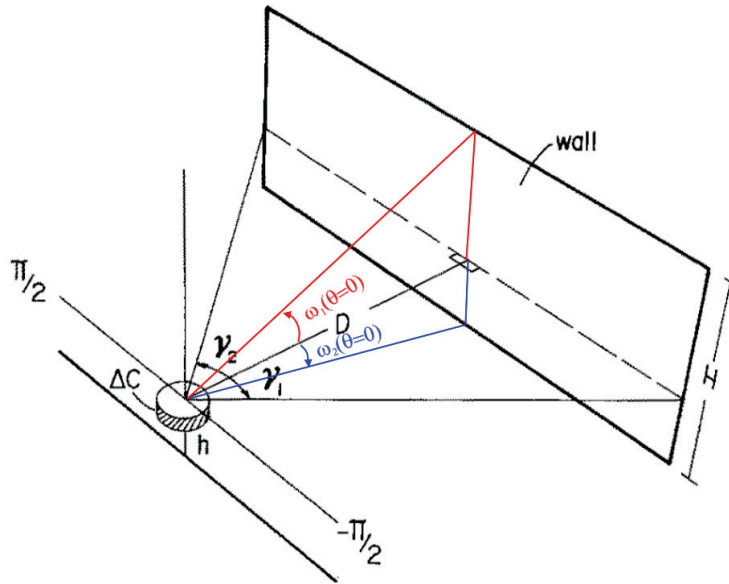
Figure A-1. Geometrical arrangement of the pedestrian (represented by a cylinder) and a building wall, **showing an infinitesimal slice ΔC of the cylinder at height h above ground and at distance D from a wall of height H. Adapted from Johnson and Watson (1984).**

The view factor from the slice side wall to the entire building wall (EBW) is

$$F_{\Delta C \to EBW} = F_{\Delta C \to UBW} + F_{\Delta C \to LBW} . \tag{A-15}$$

Applying Eq. (A-12), the view factor from cylinder side wall to the entire building wall is

$$F_{\text{C} \to \text{EBW}} = \overline{F_{\Delta\text{C} \to \text{UBW}}} + \overline{F_{\Delta\text{C} \to \text{LBW}}} \ . \tag{A-16}$$

$F_{\text{C} \to \text{EBW}}$ is calculated for each of the 10 building walls seen by the pedestrian (Figure 2).

A.1.3.   View factors from cylinder side wall to sky and ground

If the slice side wall sees N building walls, the view factors from the slice side wall to all wall regions above the slice (all UBWs) and all wall regions below the slice (all LBWs) will be

$$F_{\Delta\text{C} \to \text{all UBWs}} = \sum_{j=1}^{N} F_{\Delta\text{C} \to \text{UBW},j} \tag{A-17}$$

and

$$F_{\Delta\text{C} \to \text{all LBWs}} = \sum_{j=1}^{N} F_{\Delta\text{C} \to \text{LBW},j} \tag{A-18}$$

respectively, where j indexes the building walls.

The slice side wall has equal views of its upper hemisphere (UH, meaning everything above the slice) and its lower hemisphere (LH, meaning everything below the slice). Since the view factor from the slice side wall to the entire sphere is unity,

$$F_{\Delta\text{C} \to \text{UH}} = F_{\Delta\text{C} \to \text{LH}} = \tfrac{1}{2} \ . \tag{A-19}$$

The slice's upper hemisphere comprises the sky and all building wall surfaces above the slice (all UBWs), while its lower hemisphere comprises the ground and all building wall surfaces below the slice (all LBWs). Thus, the view factors from the slice side wall to the sky and to the ground are

$$F_{\Delta\text{C} \to \text{sky}} = F_{\Delta\text{C} \to \text{UH}} - F_{\Delta\text{C} \to \text{all UBWs}} \tag{A-20}$$

and

$$F_{\Delta\text{C} \to \text{ground}} = F_{\Delta\text{C} \to \text{LH}} - F_{\Delta\text{C} \to \text{all LBWs}} \tag{A-21}$$

respectively. Applying Eq. (A-12), the view factors from the cylinder side wall to the sky and to the ground are

$$F_{\text{C} \to \text{sky}} = \overline{F_{\Delta\text{C} \to \text{sky}}} = F_{\Delta\text{C} \to \text{UH}} - \overline{F_{\Delta\text{C} \to \text{all UBWs}}} \tag{A-22}$$

and

$$F_{\text{C}\to\text{ground}} = \overline{F_{\Delta\text{C}\to\text{ground}}} = F_{\Delta\text{C}\to\text{LH}} - \overline{F_{\Delta\text{C}\to\text{all LBWs}}} \quad , \tag{A-23}$$

respectively.

A.2. View factors from top and bottom plates to wall, sky, and ground

The view factor from the top plate to one entire building wall is

$$F_{\text{top plate}\to\text{EBW}} = \frac{1}{\pi} \int_{\gamma_1}^{\gamma_2} \int_0^{\omega_3} \cos\phi \sin\phi \; d\phi \; d\theta \,, \tag{A-24}$$

where $\omega_3 = \tan^{-1}\left(\frac{H-H_{\text{body}}}{D}\cos\theta\right)$. Since the top plate sees only the sky and the N building walls, $F_{\text{top plate}\to\text{ground}} = 0$, and the view factor from the top plate to the sky is the view factor from the top plate to the entire sphere (unity) minus the sum of its view factors to each entire building wall:

$$F_{\text{top plate}\to\text{sky}} = 1 - \sum_{j=1}^{N} F_{\text{top plate}\to\text{EBW},j} \;. \tag{A-25}$$

The cylinder's bottom plate sees only the ground, so $F_{\text{bottom plate}\to\text{ground}} = 1$, $F_{\text{bottom plate}\to\text{sky}} = 0$, and $F_{\text{bottom plate}\to\text{any wall}} = 0$.

A.3. View factors from entire cylinder to wall, sky, and ground

Consider a generic surface E with M elements denoted $\text{E}_1\ldots\text{E}_M$. If the view factor from some surface B to element E_i is $F_{\text{B}\to\text{E},i}$, the view factor from surface B to surface E will be

$$F_{\text{B}\to\text{E}} = \sum_{i=1}^{M} F_{\text{B}\to\text{E},i} \;. \tag{A-26}$$

Applying view factor reciprocity [Eq. (A-9)] to each side of Eq. (A-26) and rearranging yields

$$F_{\text{E}\to\text{B}} = \frac{1}{A_{\text{E}}} \sum_{i=1}^{M} A_{\text{E},i} \; F_{\text{E},i\to\text{B}} \;. \tag{A-27}$$

If the body of the pedestrian is represented by the surface of the cylinder, the view factor from the body to surface B (entire wall j, sky, or ground) is

$$F_{\text{body}\to\text{B}} = \frac{A_{\text{C}} F_{\text{C}\to\text{B}} + A_{\text{plate}} F_{\text{top plate}\to\text{B}} + A_{\text{plate}} F_{\text{bottom plate}\to\text{B}}}{A_{\text{body}}} \,, \tag{A-28}$$

where the cylinder's top and bottom plates each have surface area $A_{\text{plate}} = \pi\, r^2$, and the cylindrical pedestrian has surface area $A_{\text{body}} = A_C + 2{\times}A_{\text{plate}}$.